Research Article | Vol. 8, No. 6 | 1 Jun 2017 | BIOMEDICAL OPTICS EXPRESS 2896
Biomedical Optics EXPRESS

Multispectral oximetry of murine tendon microvasculature with inflammation

MARIEKE A. VAN DER PUTTEN,[1] JAMES M. BREWER,[2] AND ANDREW R. HARVEY[1,*]

[1]*School of Physics & Astronomy, University of Glasgow, G12 8QQ, UK*
[2]*Institute for Infection, Immunity & Inflammation, University of Glasgow, G12 8QQ, UK*
[*]*andy.harvey@glasgow.ac.uk*

Abstract: We report a novel multispectral imaging technique for localised measurement of vascular oxygen saturation (SO_2) *in vivo*. Annular back-illumination is generated using a Schwarzchild-design reflective objective. Analysis of multispectral data is performed using a calibration-free oximetry algorithm. This technique is applied to oximetry in mice to measure SO_2 in microvasculature supplying inflamed tendon tissue in the hind leg. Average SO_2 for controls was 94.8 ± 7.0 % (N = 6), and 84.0 ± 13.5 % for mice with inflamed tendon tissue (N = 6). We believe this to be the first localised measurement of hypoxia in tendon microvasculature due to inflammation. Quantification of localised SO_2 is important for the study of inflammatory diseases such as rheumatoid arthritis, where hypoxia is thought to play a role in pathogenesis.

OCIS codes: (110.4234) Multispectral and hyperspectral imaging; (170.0110) Imaging systems; (170.1470) Blood or tissue constituent monitoring; (170.3880) Medical and biological imaging.

References and links

1. H. K. Eltzschig and P. Carmeliet, "Hypoxia and inflammation," N. Engl. J. Med. **364**(20), 656–665 (2011).
2. P. C. Taylor and B. Sivakumar, "Hypoxia and angiogenesis in rheumatoid arthritis," Curr. Opin. Rheumatol. **17**(3), 293–298 (2005).
3. D. Mordant, I. Al-Abboud, G. Muyo, A. Gorman, A. Sallam, P. Rodmell, J. Crowe, S. Morgan, P. Ritchie, A. R. Harvey, and A. I. McNaught, "Validation of human whole blood oximetry, using a hyperspectral fundus camera with a model eye," Invest. Ophthalmol. Vis. Sci. **52**(5), 2851–2859 (2011).
4. H. C. Hendargo, Y. Zhao, T. Allenby, and G.M. Palmer, "Snap-shot multispectral imaging of vascular dynamics in a mouse window-chamber model," Opt. Lett. **40**(14), 3292–3295 (2015).
5. F. C. Delori, "Noninvasive technique for oximetry of blood in retinal vessels," Appl. Opt. **27**(6), 1113–1125 (1988).
6. J. M. Beach, K. J. Schwenzer, S. Srinivas, D. Kim, and J. S. Tiedeman, "Oximetry of retinal vessels by dual-wavelength imaging: calibration and influence of pigmentation," J. Appl. Physiol. **86**(2), 748–758 (1999).
7. T. R. Choudhary, D. Ball, J. Fernandez Ramos, A. I. McNaught, and A.R. Harvey, "Assessment of acute mild hypoxia on retinal oxygen saturation using snapshot retinal oximetry," Invest. Ophthalmol. Vis. Sci. **54**(12), 7538–7543 (2013).
8. D. J. Mordant, I. Al-Abboud, G. Muyo, A. Gorman, A. R. Harvey, and A. I. McNaught, "Oxygen saturation measurements of the retinal vasculature in treated asymmetrical primary open-angle glaucoma using hyperspectral imaging," Eye **28**, 1190–1200 (2014).
9. W. R. Johnson, D. W. Wilson, W. Fink, M. Humayun, and G. Bearman, "Snapshot hyperspectral imaging in ophthalmology," J. Biomed. Opt. **12**(1), 014036 (2014).
10. J. V. Kristjansdottir, S. H. Hardarson, G. H. Halldorsson, R. A. Karlsson, T. S. Eliasdottir, and E. Stefansson, "Retinal oximetry with a scanning laser ophthalmoscope," Invest. Ophthalmol. Vis. Sci. **55**(5), 3120–3126 (2014)
11. L. C. Clark and C. Lyons, "Electrode systems for continuous monitoring in cardiovascular surgery," Ann. N. Y. Acad. Sci. **102**, 29–45 (1962).
12. P. M. Gewehr and D. Delpy, "Optical oxygen sensor based on phosphorescence lifetime quenching and employing a polymer immobilised metalloporphyrin probe," Med. Biol. Eng. Comput. **31**, 2–21 (1993).
13. A. Rajaram, S. Ioussoufovitch, L. B. Morrison, K. St Lawrence, T. Lee, Y. Bureau, and M. Diop, "Joint blood flow is more sensitive to inflammatory arthritis than oxyhemoglobin, deoxyhemoglobin, and oxygen saturation," Biomed. Opt. Express **7**(10), 3843–3854 (2016).
14. A. H. Hielscher, K. K. Hyun, L. D. Montejo, S. Blaschke, U. J. Netz, P. A. Zwaka, G. Illing, G. A. Muller, and J. Beuthan, "Frequency-domain optical tomographic imaging of arthritic finger joints," IEEE Trans. Med. Imaging **30**(10), 1725–1736 (2011).
15. I. A. Artyukov, "Schwarzschild objective and similar two-mirror systems," Short-Wavelength Imaging and Spectroscopy Sources, Proc. of SPIE **8678**, 86780A1–A6 (2012).

#286568 https://doi.org/10.1364/BOE.8.002896
Journal © 2017 Received 10 Feb 2017; revised 13 Apr 2017; accepted 24 Apr 2017; published 8 May 2017

Biomedical Optics EXPRESS

16. P. I. Rodmell, J. A. Crowe, A. Gorman, A. R. Harvey, G. Muyo, D. J. Mordant, A. I. McNaught, and S. P. Morgan, "Light path-length distributions within the retina," J. Biomed. Opt. **19**(3), 036008 (2014).
17. M. J. M. Fischer, S. Uchida, and K. Messlinger, "Measurement of meningeal blood vessel diameter in vivo with a plug-in for ImageJ," Microvasc. Res. **80**(2), 258–266 (2010).
18. M. A. van der Putten, L. E. MacKenzie, A. L. Davies, J. Fernandez-Ramos, R. A. Desai, K. J. Smith, and A. R. Harvey, "A multispectral microscope for *in vivo* oximetry of rat dorsal spinal cord vasculature," Physiol. Meas. **38**, 205–218 (2017).
19. M.H. Smith, K. R. Denninghoff, A. Lompado, and L. W. Hillman, "Effect of multiple light paths on retinal vessel oximetry," Appl. Opt. **39**(7), 1183–1193 (2000).
20. S. Prahl, "Optical Absorption of Haemoglobin," *http://omlc.org/spectra/hemoglobin/index.html*, Oregan Medical Laser Centre (1999), accessed April 2017.
21. M. Friebel, J. Helfmann, U. Netz, and M. Meinke, "Influence of oxygen saturation on the optical scattering properties of human red blood cells in the spectral range 250 to 2000 nm," J. Biomed. Opt. **14**(3), 034001 (2009).
22. C. Hanning and J. M. Alexander-Williams, "Pulse oximetry: A Practical Review," BMJ **311**, 367–360 (1995).
23. P. Gaehtgens, "Distribution of flow and red cell flux in the microcirculation," Scand. J. Clin. Lab. Invest. **41**(1), 83–87 (1981).
24. D. Schweitzer, L. Leistritz, M. Hammer, M. Scibor, U. Bartsch, and J. Strobel, "Calibration-free measurement of the oxygen saturation in retinal vessels of men," Ophthalmic Technologies V, Proc. SPIE **3293**, 210–218 (1995).
25. R. H. Byrd, R. B. Schnabel, and G. A. Shultz, "A Trust Region Algorithm for Nonlinearly Constrained Optimization," SIAM J. Numer. Anal. **24**(5), 1152-1170 (1987).
26. J. Necas and L. Bartosikova, "Carrageenan: a review," Vet. Med. Czech **58**(4), 187–205 (2013).
27. C. J. Morris, "Carrageenan-Induced Paw Edema in the Rat and Mouse," Inflammation Protocols: Methods Mol. Biol. **225**(2), 115–121 (2003).
28. C. G. Ellis, M. L. Ellsworth, and R. N. Pittman, "Determination of red blood cell oxygenation in vivo by dual video densitometric image analysis," Am. J. Physiol. **258**(4), 1216–1223 (1990).
29. L. E. MacKenzie, T. R. Choudhary, A. I. McNaught, and A. R. Harvey, "*In vivo* oximetry of human bulbar conjunctival and episcleral microvasculature using snapshot multispectral imaging," Exp. Eye Res. **149**, 48-58 (2016).
30. E. Salomatina and A. N. Yaroslavsky, "Evaluation of the in vivo and ex vivo optical properties in a mouse ear model," Phys. Med. Biol. **53**(11), 2797–2807 (2008).
31. D. L. Asquith, A. M. Miller, I. B. McInnes, and F. Y. Liew "Animal models of rheumatoid arthritis," Eur. J. Immunol. **39**(8), 2040-2044 (2009).
32. K. Briely-Saebo and A. Bjornerud, "Accurate de-oxygenation of ex vivo whole blood using sodium Dithionite," Proc. Intl. Soc. Mag. Reson. Med. **8**, 2025 (2000).
33. M. Friebel, J. Helfmann, and M. C. Meinke, "Influence of osmolarity on the optical properties of human erythrocytes," J. Biomed. Opt. **15**(5), 055005 (2010).

1. Introduction

An adequate supply of oxygen is critical to the normal and healthy function of cells and tissues. The microvasculature, comprised of the smallest blood vessels in the body, is the means by which oxygen is delivered. Hypoxia, a state of insufficient oxygen, may be caused either by a decreased supply of oxygen delivered by the vasculature, or increased demand in the tissue. The link between inflammation and tissue hypoxia is well established [1], with molecular markers for hypoxia and associated angiogenesis linked to chronic immune-related disease such as rheumatoid arthritis (RA) [2]. It is not known, however, what role hypoxia plays in the progression of RA, where hypoxia originates in the affected joint, or to what extent hypoxia may be suitable as a proxy biomarker of RA and inflammation for diagnostic purposes.

Multispectral oximetry can provide highly localised quantification of blood oxygen saturation (SO_2), owing to the distinct spectral characteristics of oxygenated and deoxygenated haemoglobin [3, 4]. Much of the research to date into techniques for *in vivo* vascular oximetry have focused on the eye, specifically the retina where it is of interest in the study of conditions such as glaucoma, diabetic retinopathy and retinopathy of prematurity [5–9]. These diseases are often related to dysfunctional supplies of blood oxygen, and as such the study of SO_2 in retinal vasculature can provide useful information regarding the health of the individual. The prevalence of oximetry in the eye is perhaps owed to the ease with which retinal vessels can be imaged non-invasively, using modified slit lamps and ophthalmoscopes, for example [10]. Hypoxia associated with inflammatory disease is generally localised to the affected area; in the

Biomedical Optics EXPRESS

case of RA, it is the tendons and joints which become inflamed and hypoxic [1]. Obtaining localised *in vivo* measurements of SO_2 in tendon tissue is naturally more challenging as it is not optically accessible due to overlaying layers of skin and other tissue. Bulk oximetry modalities such as Clark electrodes and fibre-optic oxygen probes may be used for interrogation of oxygen levels in deep tissue [11, 12]. Previous studies of joints affected by RA carried out using diffuse optical spectroscopy (DOS) and diffuse optical tomography (DOT) [13, 14] used transmitted illumination to measure the absorption and scattering properties of the joint, to hence distinguish between healthy and affected joints. However, the resolution of the measurements is poor and does not provide absolute values of vascular oxygen saturation. Multispectral imaging oximetry provides highly localised SO_2 information specific to individual blood vessels, at a much higher resolution than achievable with bulk probe or DOT measurements. Future work will investigate what the potential diagnostic advantages are to using these highly localised measurements compared with bulk measurements. Regardless, localised oximetry is desirable for helping to provide a greater understanding of the spatiotemporal manifestation of hypoxia in inflamed or diseased tissue.

In this paper, we describe multispectral imaging oximetry and analysis of oxygen saturation in the tendon microvasculature of the mouse hind leg, comparing control and inflamed mouse tendons. In this case, optical access was achieved by surgical excision of the skin overlying tendon tissue in the mouse hind leg. This study provides a basis upon which to further develop minimally invasive oximetry techniques using microendoscopic probes, which will be highly transferable for a range of *in vivo* applications.

2. Multispectral imaging and analysis technique

2.1. Imaging system and illumination

A schematic for the imaging system is shown in Fig. 1. Spectrally tunable illumination is provided by a white-light supercontinuum source (Fianium SC400) coupled to an acousto-optic tunable filter (AOTF). An oscillating polymer membrane (Optotune Laser Speckle Reducer 3005) was used to reduce spatial coherence and associated image speckle.

A Schwarzchild-type reflective objective [15] (Thorlabs LMM-40X-UVV) and imaging lens (f = 200 mm) provided 40X magnification, corresponding to 0.165 μm per pixel. The reflective objective provides achromatic imaging and also a means to simultaneously employ annular illumination as is commonly used in capillaroscopy. Annular illumination simplifies and improves the accuracy of the oximetry algorithm; with annular illumination, back-scattered light is eliminated and detected light arises only from single-pass absorption through a blood vessel. This concept has been validated for retinal vessels by Rodmell et al [16]. Simplification and improvement in the accuracy of the oximetry algorithm is hence achieved as described in section 2.2.

Using a reflective objective to generate annular illumination is straightforward. When collimated light is incident on the back aperture of a Schwarzchild-type reflective objective, as with any lens, a focused spot is formed at the focal plane of the objective. If the illumination focus is offset from this focal plane, however, the defocused spot is approximately annular in shape. The central portion of the beam is blocked by the primary mirror of the objective, resulting in a shadow which creates an illumination pattern as shown in Fig. 1(C). A planoconvex lens (f = 80 mm, L3 in Fig. 1(A), was used to offset the focus of the illumination such that this annulus was just larger than the field of view. This resulted in an inner diameter of the annulus of approximately 240 μm.

Most of the light incident on the primary mirror of the objective is deflected towards the secondary mirror before coming to a focus. However, a small central portion of the incident beam is directly back-reflected from the centre of the primary mirror, causing loss of contrast and interference patterns in the image. To prevent this, a beam block was introduced at the

Biomedical Optics EXPRESS

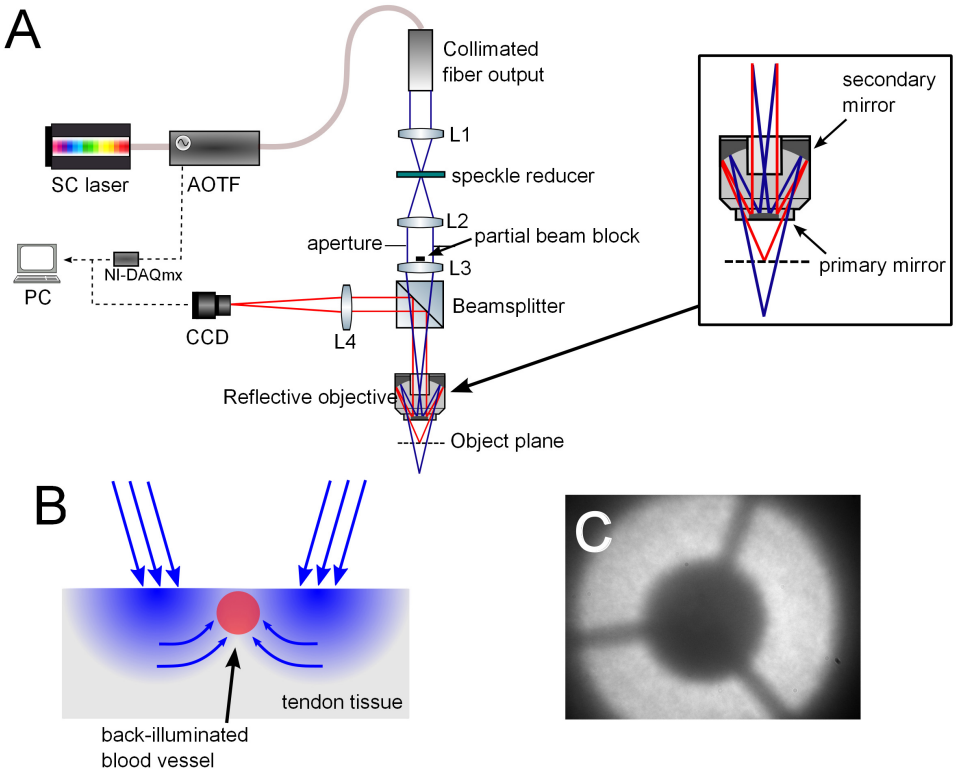

Fig. 1. **A.** Schematic of imaging setup. The illumination path is shown in blue, and imaging path in red. Image acquisition and AOTF switching was controlled by means of a National Instruments data acquisition toolbox (NI-DAQmx) and custom Labview interface. SC = supercontinuum; AOTF = acousto-optic tunable filter; L1, L2, L3 = lenses 1, 2, 3 respectively; L4 = imaging lens. The partial beam block prevents the central region of the illumination path being back-reflected toward the CCD and interfering with the imaging path. **B.** Illustration of annular light diffusion through tissue for back-illumination of the vasculature. **C.** Image of illumination pattern generated by off-setting the focus of the illumination from the focal plane of the reflective objective. For imaging, the optics are configured such that the central dark region of the pattern is just larger than the field of view.

Biomedical Optics EXPRESS

centre of the illumination beam, which was placed directly above lens L3 (as depicted in Fig. 1(A)). This effect is less of an issue for reflective objectives with anti-reflective coating at the centre of the primary mirror.

For multispectral imaging of the microvasculature, an isosbestic wavelength (420 nm) and 5 oxygen-sensitive wavelengths were chosen; 410 nm, 430 nm, 435 nm, 440 nm and 450 nm. The extinction coefficients of haemoglobin are highest in this visible blue region, which is desirable to provide sufficient contrast when imaging the smallest blood vessels. The strong absorption of light by blood in this wavelength range offers sufficient contrast even through thin layers of overlaying tissue. Further, the difference between the coefficients for oxygenated and deoxygenated haemoglobin at these wavelengths is large enough to allow for accurate oximetry of these small vessels; optical densities of the vasculature will change significantly with oxygen saturation over this range. Previous oximetry studies performed on retinal blood vessels *in vivo* have employed wavelengths in the green and red regions [6,7], however the microvasculature is highly transparent in this region due to lower extinction coefficients. A multispectral dataset of a single scene consists of a set of images recorded at each waveband. Data acquisition was controlled by a custom LabVIEW interface, which switched the waveband being transmitted by the AOTF, and triggered the CCD image capture. The total acquisition time for one dataset was less than 2 seconds. The CCD exposure at each waveband (200 ms for 410 nm - 440 nm, 100 ms for 450 nm because of source brightness) contributes to this time, as well as the read-write speed of the computer hard drive.

2.2. Oximetry algorithm

Although relative oximetry is possible with just two wavelengths, the algorithm used here for multispectral data analysis is insensitive to vessel diameter, pigmentation and scattering. As multispectral imaging provides more measurements than unknowns, a least-squares error fit enables absolute oxygenation measurements. The algorithm first involves co-registering the six images at each waveband. Semi-automatic vessel tracking is then performed to determine coordinates along vessels appropriate for analysis. To quantify light transmission through the blood vessels at each waveband, multiple line profiles are taken across each vessel in an image, perpendicular to each pair of successive image coordinates along the vessel. The transmission of light through the vessel is defined as $T = \frac{I}{I_o}$, where I_o is the background intensity and I is the intensity of light transmitted through the vessel. An estimate of I_o is obtained from a linear fit to each line profile, ignoring the central vessel pixels. A second order polynomial fit is then applied to the central region of the line profile, from which the minimum, I, is estimated. Transmission is calculated at every point along the vessel, and at every waveband, producing an experimental transmission profile $T(\lambda)$. The diameter of the vessel is also determined using these line profiles and the method described by Fischer et al., (2010) [17].

To determine values for SO_2, we implemented an analytical model for optical transmission of light through blood vessels. The data would then be applied to the model in a series of iterative nonlinear least-squares fits in order to extract unknown parameters, including SO_2. Based on the modified Lambert-Beer law, previous work by van der Putten et al. [18] and Smith et al. [19], the optical transmission of a blood vessel can be written as:

$$T(\lambda) = s\,(1-K)\cdot 10^{-\left(C_{Hb}(\lambda)\eta d\left[\left(\varepsilon_{HbO_2}(\lambda)-\varepsilon_{Hb}(\lambda)\right)SO_2+\varepsilon_{Hb}(\lambda)\right]+\left[\left(\mu'_{HbO_2}(\lambda)-\mu'_{Hb}(\lambda)\right)SO_2+\mu'_{Hb}(\lambda)\right]\eta d\right)}+K \tag{1}$$

where d is vessel diameter; $\varepsilon_{HbO_2}(\lambda)$ and $\varepsilon_{Hb}(\lambda)$ are molar extinction coefficients of oxygenated and deoxygenated haemoglobin respectively; and $\mu'_{HbO_2}(\lambda)$ and $\mu'_{Hb}(\lambda)$ are empirical values for the reduced scattering coefficients. In this work we take values for extinction coefficients from Prahl (1999) [20] and scattering coefficients from Friebel et al., 2009 [21]. These

Biomedical Optics EXPRESS

coefficients have been derived empirically using *ex vivo* blood, and therefore our technique is accurate across all oxygen saturation values, unlike traditional pulse oximetry techniques which are calibration-based and typically unreliable below oxygenations of 70% [22]. In theory it is necessary to integrate over the illumination spectrum to achieve effective values for extinction and reduced scattering coefficients for oxygenated and deoxygenated haemoglobin. However, the nominal bandwidth of the AOTF is 2 nm, and for the purposes of the analysis the illumination is considered to be monochromatic. The calculated concentration of haemoglobin in blood, C_{Hb}, was allowed to vary from an accepted average value of 160 M/liter, as vessel size and shape is likely to influence haemoglobin concentration [23]. K is an unknown parameter, between 0 and 1, which is introduced to compensate for contrast reduction which can occur due to changes in tissue thickness above the vessel, and optical scattering in the imaging system. Contrast reduction is modelled as an additive intensity component I_c to both I and I_o, where $K = \frac{I_c}{I_o+I_c}$. The unknown parameter s accounts for the light collection geometry [24].

The factor η represents the proportion of single-pass and double-pass illumination [19]. For purely single-pass absorption, η will be 1, whilst for double-pass absorption, η would be equal to 2. The annular illumination configuration previously described ensured that light illuminating the field of view will be diffuse, having scattered through the tissue from the surrounding annulus of illumination. We assume that only light having undergone a single transmission will reach the detector and so $\eta = 1$, reducing the number of free variables. This illumination configuration also ensures that negligible back-scattered light would be detected, and so this component was not included in the model.

The iterative fits of the model to the data were employed using a trust-region reflective algorithm [25]. The fits were performed by first averaging the experimentally obtained transmission profile $T(\lambda)$ over the length of the vessel, and performing an initial fit to give preliminary values for s, SO_2, K, and C_{Hb}. Three further fits were applied in which s, K and SO_2 were allowed to vary respectively, with all other parameters held constant to its most recently determined value. This method proved to be robust with calculated SO_2 approximately constant along each vessel; the average standard deviation of SO_2 for all vessels was determined to be 2.3 %. The goodness of fit was assessed by quantifying the coefficient of determination (R^2) of the final fit producing the SO_2 parameter. The results for particularly noisy data, where $R^2 < 0.9$, were excluded from further analysis.

3. *In vivo* imaging of tendon microvasculature

3.1. Methods

All procedures involving the use of living animals were carried out in accordance with UK Home Office guidelines. The study involved 13 female inbred BALB/c mice (18-25 g, 6-8 weeks old, *Harlan*). Six mice were used as controls, and inflammation was induced in another six mice using λ-carrageenan [26]. The remaining mouse was used for a kinetic study of SO_2 as a function of inflammation. Carrageenan is a group of complex polysaccharides, the lambda form of which is injectable and induces an acute inflammatory response, peaking 5 hours post-inoculation [27]. 25 µl of 1% λ-carrageenan solution in sterile phosphate-buffered saline was injected into the mouse footpad of the left hind leg. Inflammation of the footpad was validated by measuring footpad thickness prior to injection, and again 5 hours post-injection, prior to imaging. Footpad thickness increased in this time from an average of 1.6 ± 0.1 mm to 3.0 ± 0.3 mm.

All mice were anaesthetized prior to surgery with fentanyl-fluanisone (Hypnorm), midazolam (Hypnovel) and water (1:1:2 by volume) at a dose of 10 µl/g injected intraperitoneally. The peroneus longus tendon, proximal to the calcaneus in the hind leg, was then surgically exposed by removal of superficial skin layers, which can enable diffusion of oxygen into the blood vessels through air. We used a layer of oxygen-impermeable plastic film placed in contact with

Biomedical Optics EXPRESS

the exposed tendon tissue to prevent oxygen diffusion, as used in previous studies to isolate blood vessels from oxygen in the atmosphere [28]. This is an important issue for invasive *in vivo* oximetry; exposure of blood vessels to air will result in an increase in SO_2 with respect to normal values, as has previously been observed in the human sclera [29]. The film also prevents the tissue from drying out over the course of the experiment.

The mouse was placed on the microscope stage and heat pad, which was kept at approximately 37°C. The hind leg was secured to a small block using surgical tape and *Vetbond* tissue adhesive. To reduce motion artefacts due to mouse breathing, the leg was kept mechanically stabilised with respect to the body using a custom, 3D-printed bridge. Setting up the mouse in this manner reduced motion to an acceptable degree required for time-sequential multispectral imaging. A series of spectral datasets were recorded for each mouse tendon over the course of several minutes.

3.2. Results and discussion

Image data was processed using the algorithm described in section 2.2. For each mouse, a range of vessels were selected for analysis. Fig. 2 shows an illustrative example of a tendon microvasculature image and the calculated SO_2 map. The average values for SO_2 produced for each mouse are shown in Fig. 3, along with the overall average of all results for control and inflamed mice. These values were determined to be 94.8 ± 7.0 % for control SO_2, and 84.0 ± 13.5 % for inflamed SO_2 respectively (average ± standard deviation). Performing a two-sample t-test, the difference is highly significant ($p < 0.001$). This suggests that average SO_2 levels are lower in the inflamed tendon vasculature than for the controls. The link between inflammation and hypoxia is well established, so this result is not surprising, however we believe this to be the first quantification of *localised* hypoxia in the vasculature of inflamed tendons.

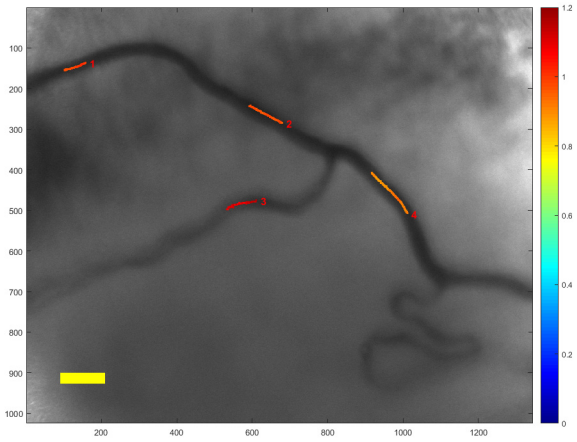

Fig. 2. Illustrative image of tendon microvasculature and SO_2 map. The colour bar represents SO_2, and each vessel length analysed is numbered and labelled on the image. The scale bar represents 20 μm.

As well as a comparison of control and inflamed tendons, an additional oximetry study was performed on a mouse tendon post mortem as validation that the technique is sensitive to changes in blood oxygenation. It is known that rapid deoxygenation of the vasculature occurs post mortem due to local metabolism of oxygen by cells which continues after death [30]. For one case, a mouse was euthanised whilst secured to the imaging stage, and data was acquired 5 minutes post mortem, at which point the blood vessels are assumed to be highly deoxygenated. It was found, as shown in Fig. 4, that calculated SO_2 decreased in this time from 71.9 ± 7.4 %

Biomedical Optics EXPRESS

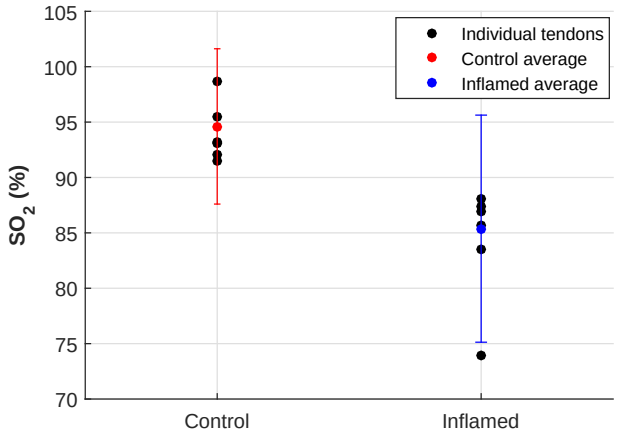

Fig. 3. Oximetry of control and inflamed (5-6 hours post λ-carrageenan inoculation) mouse tendon vasculature, shown as values for individual tendons averaged over multiple vessels. The overall average for control and inflamed tendons are shown in red and blue respectively ± standard deviation between tendons.

to 48.2 ± 8.2 %, further supporting the responsivity of the technique to oxygen saturation.

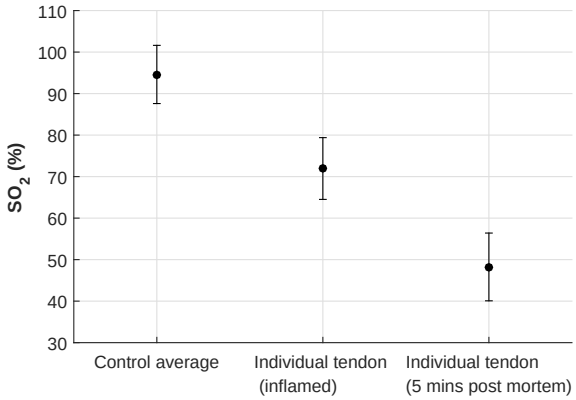

Fig. 4. Comparison of overall control SO_2 (average over all tendons ± standard deviation), average inflamed SO_2 for an individual mouse , and SO_2 of the same tendon post mortem (both averaged over all vessels within tendon ± standard deviation)

Finally, for one additional mouse, a kinetic analysis was performed to investigate SO_2 as a function of time after inoculation with λ-carrageenan. As the inflammatory response peaks after 5 hours, oximetry was conducted every half hour between 1 and 5 hours post inoculation, assuming that there is a correlation between hypoxia and degree of inflammation. The results shown in Fig. 5 indicate that whilst there was considerable scatter between individual measurements at each time point, there was an overall downward trend in average SO_2 value as expected, with the Pearson correlation coefficient r = -0.63. For this correlation, the corresponding p-value = 0.095 is not low enough to be considered highly statistically significant. It may be possible that the linear correlation we have assumed between hypoxia and time since inoculation is not a valid model. As a number of vessels were analysed at each time point, the scatter seen in the figure

Biomedical Optics EXPRESS

most likely reflects the natural biological variation of SO_2 in distributed blood vessels. Previously it has not been possible to measure the variability of SO_2 between individual blood vessels in the tendon, and it may be the case that it is an inhomogeneous environment. The technical approach described here, does however provide evidence to correlate hypoxia with inflammatory disease, and provides a tool which will enable this relationship to be investigated in more detail with longitudinal studies in animal models of inflammatory disease [31].

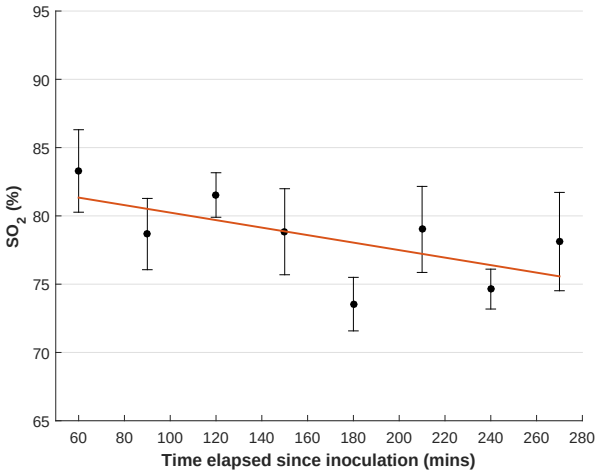

Fig. 5. Kinetic analysis of SO_2 as a function of increasing inflammation after inoculation with λ-carrageenan, mean ± standard error, r = -0.63, p = 0.095

4. Conclusion

We have developed and demonstrated a novel multispectral imaging system and analysis technique capable of performing oximetry in the microvasculature *in vivo*. We have performed the first measurements of localised microvasculature oxygen saturation in tendon tissue, and quantified hypoxia associated with an acute model for inflammation. Previously, it had been shown through bulk measurement and histological analysis that inflamed tendon tissue is hypoxic [1,2]. We have now ascertained that hypoxia is present not only in the tissue, but have also quantified it in the associated microvasculature.

We obtained physiologically plausible values for SO_2 of healthy microcirculation, and a decrease in SO_2 associated with hypoxia, as expected. We also measured reductions in SO_2 over a time course following inoculation, as the degree of inflammation increased. Additionally, a marked decrease in SO_2 of blood vessels immediately post mortem indicates that the technique is sensitive to changes in localised SO_2. However, accurate validation of the absolute values produced by the algorithm remains a challenge. There was significant scatter between individual measurements of blood vessels between different tendons, and indeed also between different blood vessels of the same tendon; the standard deviation for all control measurements was 7.0 %, and 13.4 % for the inflamed measurements. As we have studied the smallest vessels of the microvasculature, there will naturally be a spread in true oxygen saturation values across different vessels which is likely the cause of this high standard deviation. However, it is difficult to assess the extent to which this spread is caused by physiological differences or in fact caused by potential inaccuracies in the imaging and analysis process. Due to the highly localised nature of these measurements, no other methods exist for localised determination of SO_2 in the microvasculature, with which our results could potentially be compared. Options for *in vitro* validation

Biomedical Optics EXPRESS

exist, using phantoms that mimic blood vessels in tendon tissue; *in vitro* blood can be accurately deoxygenated using sodium dithionite [32]. However, this introduces problems such as increasing the osmolarity of blood, which has been shown to affect its optical properties [33]. Such a method of validation is hence questionable, as the extinction and reduced scatter coefficients employed in our model would not be correct in this case. Further work is required for accurate validation and assessment of the accuracy of the oximetry algorithm.

This is an invasive technique, with surgical removal of the skin necessary in order to achieve optical access to the tendon. Future work will pursue the incorporation of a minimally-invasive microendoscope, using a similar illumination scheme and analysis technique as presented in this paper. The microendoscope will act as an optical relay from the vasculature within the tendon to the focal plane of the microscope described here. Initial tests with this probe setup *ex vivo* indicate that the vasculature remains detectable through tissue at a working distance of 100 μm, however challenges remain in order to ensure oximetry measurements are not adversely affected by potential contact pressure. Minimally-invasive oximetry will circumvent the need for invasive surgery, and allow for the longitudinal study of SO_2 in more realistic models of RA, looking at the same mouse and vasculature over the course of several weeks. It will then be possible to determine whether correlates exist between hypoxia and conventional disease-scoring approaches. It is hoped that a greater understanding of the role that hypoxia plays in disease progression and inflammation will be gained, with the availability of localised SO_2 information previously inaccessible using bulk oximetry probes. Looking forward, with such minimally-invasive localised oximetry techniques now in development, it may be possible to perform localised measurement of SO_2 of deep tissue in humans - using hypoxia as a proxy biomarker for a range of inflammatory diseases.

Funding

Lord Kelvin Adam Smith Scholarship (LKAS), University of Glasgow.